Synthesis and characterization of amorphous mesoporous materials impregnated with Hematite (Fe_2O_3) for use in the H_2S removal

B. Rondón[a*], P. Silva[b, d], J. Arjona[a], J. Mantilla[c]

[a] Escuela de Física. Universidad Central de Venezuela (UCV), Caracas 1051, Venezuela.
[b] Centro de Física. Instituto Venezolano de Investigaciones Científicas (IVIC), Caracas 1020-A, Venezuela.
[c] Instituto de Física, Universidade Federal de Mato Grosso do Sul, Campo Grande, MS. CP. 79070-900, Brazil.
[d] Escuela Superior Politécnica del Litoral (ESPOL), Campus Gustavo Galindo - 2019, Guayaquil, Guayas, Ecuador.

*Corresponding author, E-mail: beercheba@yahoo.com

Received: 19-09-20 Accepted: 29-03-21
Published: 09-04-21

ABSTRACT
In this work, three amorphous mesoporous materials (MMD1, MMD2, and MMD3) with different structural characteristics were synthesized and impregnated with 10% of Fe_2O_3, in-order-to obtain an effective amorphous mesoporous material (MMD) for H_2S adsorption. These materials were characterized by using SEM, EDX, TEM, ICP-MS, N_2 Adsorption, and DRX. Capacity tests for H_2S adsorption were performed to evaluate its performance as adsorbents of this gas. The results showed that the MMD1 mesoporous material impregnated with Fe_2O_3 showed the highest adsorption capacity of H_2S concerning the other materials studied in this work. This material could be a good option to control environmental emissions and improve the quality of the oil and gas.

Keywords: Adsorption capacity; removal H_2S; Hematite; amorphous mesoporous; Sol-Gel.

Síntesis y Caracterización de materiales amorfos impregnados con Hematita (Fe_2O_3) para su uso en la Remoción de H_2S

RESUMEN
En este trabajo, tres materiales mesoporosos amorfos (MMD1, MMD2 y MMD3), con diferentes características estructurales, fueron sintetizados e impregnados con 10% de Fe_2O_3 a manera de obtener un material mesoporoso amorfo (MMD) efectivo para la adsorción de H_2S. Estos materiales fueron caracterizados utilizando SEM, EDX, TEM, ICP-MS, Adsorción de N_2 y DRX. Se realizaron pruebas de capacidad de adsorción de H_2S para evaluar su desempeño como adsorbente para este gas. Los resultados mostraron que el material mesoporoso MMD1 impregnado con Fe_2O_3 mostró la capacidad de adsorción de H_2S más alta en comparación con los otros materiales estudiados en este trabajo. Este material podría ser una buena opción para el control de emisiones ambientales de H_2S y mejorar la calidad del petróleo y el gas que se produce.

Palabras claves: Capacidad de adsorción, remoción de H_2S, Hematita, mesoporos amorfos, Sol-Gel.

INTRODUCTION

Industrial processes can generate toxic gases that, inhaled in large quantities could cause death [1-2]. Among these toxic gases is hydrogen sulfide (H_2S), also known as sour gas or acid gas, which is responsible for many occupational incidents due to toxic exposure, including within the oil industry. This gas caused the death of 60 workers between 2001 and 2010 [3].

The H_2S is found naturally in oil, natural gas, volcanic gases, and hot springs. It can also exist in swampy waters, lagoons or stagnant waters, drains, fishmeal or fish oil ponds, fishing boats, and sewers. The H_2S is produced by the decomposition of organic matter containing sulfides [1]. It is a flammable, colorless gas, noticeable in very low contents, and has a smell similar to rotten eggs. This gas together with carbon dioxide (CO_2) forms acid rains.

Different studies have been proposed in the scientific field in-order-to remove H_2S using porous materials such as zeolites, modified clays, activated carbon, among others, as gas adsorbents [2]. Porous materials are present in various industrial processes due to their particular characteristic of having interconnected pores or gaps, high

surface area, thermal stability that make them very useful for catalysis, adsorbents, molecular sieves, among others [4-5]. Different authors have proposed alternatives as H_2S adsorbents, such as the mesoporous SBA 3 with 5%, 10%, and 15% of ZnO content which demonstrates that the adsorption of H_2S, is influenced by the good dispersion and accessibility of metal oxide in the mesoporous matrix. [6]. Other studies report that the MCM-41 silica mesoporous with a high surface area of 1270 m^2/g and a porosity of 69% synthesized by the Sol-Gel method has a superior performance in adsorption of H_2S in wastewater which makes it an excellent adsorbent for applications in wastewater treatments [7]. The excellent oxidation properties of H_2S with a material based on three-dimensional mesoporous carbon monoliths doped with carbon nanotubes and with abundant surface nitrogen species as active sites is attributed to the interconnected network of the macro and mesopore channels and to a large amount of nitrogen as structural defects that allowed desulfurization of 490 g_{sulf}/Kg_{cat} [8]. Li et al. [9] prepared mesoporous silicon materials type SBA-16, MCM-48 and KIT-6 impregnated with different percentages of zinc oxide (ZnO) to investigate the best H_2S removal capacity and found that the H_2S adsorption capacity varies according to the order KIT-6> MCM-48> SBA-16 and is related to pore size. They also found that the best loading capacity for the ZnO was 30% supported on MCM-48 and KIT-6 followed by 20% on SBA-16 showing that for increases in the percentage the adsorbent capacity decreases due to the agglomeration of the ZnO.

In this work, three different mesoporous materials were synthesized and impregnated with 10% w/w of Fe_2O_3 with the aim of obtain mesoporous material effective for the adsorption of H_2S for the control of H_2S emissions to the environment, the quality of the crude oil, and the gas produced in the oil industries. These mesoporous materials were characterized with different analysis techniques to know their surface, morphological and structural properties; and their capacity in the adsorption of H_2S was also evaluated.

MATERIALS AND METHODS

Preparation.

The amorphous mesoporous samples were prepared using the Sol-Gel method in an acid medium. The amorphous mesoporous materials MMD1 and MMD2 were prepared using surfactants as the structure-directing agent and sodium silicate as the source of silica. The DETEX-15 surfactant and a natural surfactant obtained from the Parapara-fruit (Sapindus Saponaria) were used for preparing the MMD1 and MMD2 matrix, respectively. The synthesis was carried out preparing a solution by mixing distilled water with sodium silicate Glassven brand (Na_2SiO_3, 29.6% purity of SiO_2, 9.3% Na_2O, and 61% H_2O) and then adding to this solution the mix of 5.2 g of surfactant, 41 g of distilled water, and 10.2 g of Fischer Scientific sulfuric acid (H_2SO_4), purity 98%, at 22%. The gel was dried for 8 hours at 97°C and calcined from room temperature to 550°C for 8 h.

The amorphous mesoporous material 3 (MMD3) was prepared by mixing 10.2 g of a Y type zeolite PQ Corp. brand, 10 g of Riedel-de-Haën TEOS, 99% purity, and 25.8 g of ethanol for a first solution. The second and third solutions were prepared by mixing 22.7 g of Sigma Aldrich citric acid, 99% purity with 39.3 g of distilled water, and 2 g of Riedel-de-Haën Aluminum Nitrate $Al(NO_3)$, 99% purity with 10.1 g distilled water, respectively. Once the solutions were prepared, the second and third solutions were added dropwise to the first solution and stirring for 30 min. Then, the mixture solution is kept at 60°C and rest for 24 h and calcined at 600°C in an air-stream with a heating rate of 2.5°C/min. The incorporation of iron oxide Fe_2O_3 in a concentration of 10% in weight was carried out by using the wet impregnation method with the Riedel-de-Haën Iron Nitrate $Fe(NO)_3$, purity of 98%, as the precursor. The

samples were dried at 80°C for 24 hours and then calcined at 550°C for 4 hours.

Characterization.

The morphological characterization was made using scanning electron microscopy (SEM) and the quantification of elements present was performed using X-ray Dispersive Spectroscopy (EDX). Both techniques were performed with an FEI microscope, Quanta FEG 250 model. Mass of Fe_2O_3 in %w/w was obtained through the Mass Spectrometry with Plasma Coupled ICP-MS with a Varian ICP-OES equipment, Model MPX. Transmission electron microscopy (TEM) images were obtained with a high-resolution electron microscope JEOL, model JEM 2100. Textural properties were obtained by adsorption/desorption of nitrogen using a Micromeritics Tristar 3000 model. Pore size distribution was performed by the Barret-Joyner-Hallender (BJH) method using the desorption branch for samples MMD2 and MMD3. The average pore diameter was used for MMD1. The surface area was calculated by Brunauer-Emmett-Teller (BET). Pre-treatment was carried out on degassed samples in vacuum at 300°C for 4h.

The X-ray diffraction was used to study the structure and crystalline phases of the samples with a PANalytical Xpert Pro model with a goniometer model PW3050/6X X-ray diffractometer. The particle size from DRX was obtained using the Scherrer equation 1:

$$\tau = \frac{K\lambda}{\beta \cos\theta} \qquad (1)$$

The detector step-time was 30 s, the anode material was Copper (Cu) with a wavelength of K-α1 of 1,54060 Å, using a starting position of 5°, end position of 90°, and a detector step size of 0.02°.

Adsorption capacity tests of H_2S were performed with an experimental setup as shown in figure 1. The experimental procedure of the tests consisted of placing 0.5 g of the powder sample inside of the autoclave. Nitrogen was used to purge the line. After 2 h of stabilizing the temperature at 40°C, the N_2 was released. Then, H_2S gas was incorporated at 120 PSI pressure. Pressure, temperature, and time were recorded during the test. The H_2S adsorption capacity was calculated by pressure drops using equation 2, where C_a is the adsorption capacity, P_i is the initial pressure, P_f is the equilibrium pressure, M is the molecular weight of H_2S, M_{ads} is the mass of the sample (adsorbent) and V is the volume of the autoclave where the test was performed.

$$C_a = \frac{\frac{MV}{RT}(P_f - P_i)}{M_{ads}} \qquad (2)$$

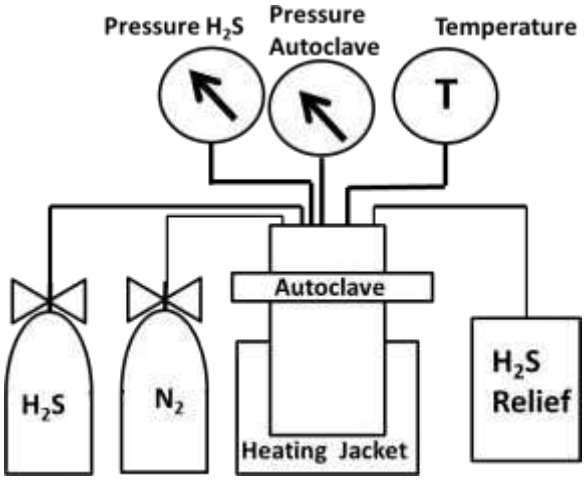

Fig. 1. Assembly and Scheme for H_2S adsorption tests.

RESULTS AND DISCUSSION

Scanning Electron Microscopy.

Figure 2A shows the SEM micrographs for the MMD1 sample. A surface with darker local areas corresponding to sites with great depth such as holes is observed. In figure 2B the MMD1-Fe_2O_3 sample is shown, a reduction in contrast in the areas related to the holes described for pure MMD1 sample is observed. This modification of the surface is associated with the presence of the oxide; since the images by backscattering electron (BSE) allow differentiating in terms of the atomic number Z the materials present in the sample [10]. There is a difference

in contrast between the substrate, which is more opaque, and some areas brighter associated with nucleation points of the oxide particles, which uniformly cover the support. From figure 2C, pure MMD2 shows a uniform surface, while for MMD2-Fe_2O_3 (figure 2D) bright areas can be observed, indicating the presence of the metal oxide in greater concentration. Figure 2E shows the MMD3-Fe_2O_3 sample, certain areas with greater brightness that indicate the presence of metal oxide particles are observed. However, low contrast is observed, which may be related to some effect of the support on the distribution of the oxides on its surface. No Z-contrast micrographs were performed for MMD3 without impregnation because the support does not show variations in terms of Z contrast.

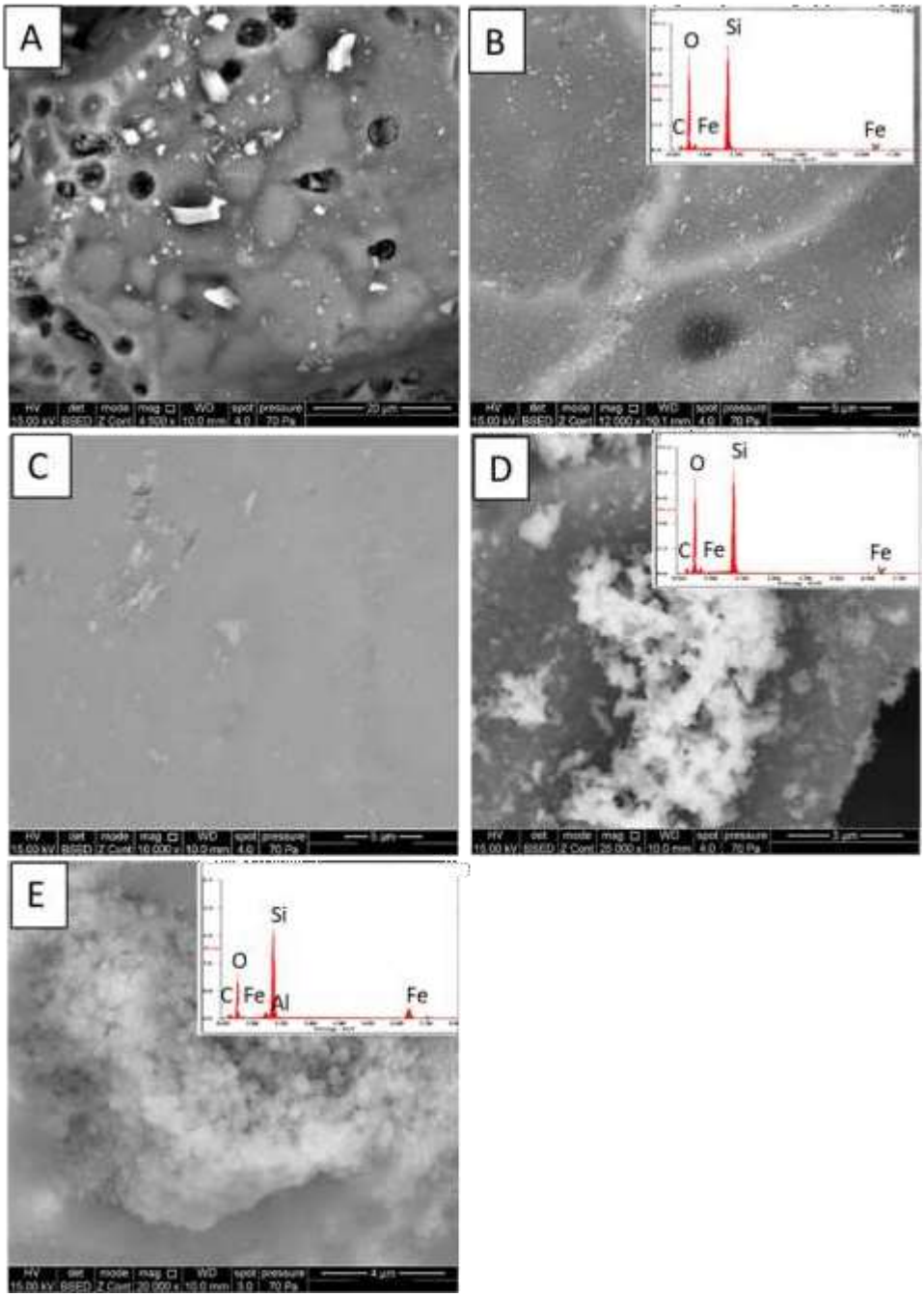

Fig. 2. SEM Image in Z contrast: pure MMD1 (A), MMD1-Fe_2O_3 (insert EDX) (B), pure MMD2 (C), MMD2-Fe_2O_3 (insert EDX) (D), MMD3-Fe_2O_3 (insert EDX) (E).

Figure 3 shows SEM micrographs for MMD2-Fe_2O_3. Particles of spherical shape uniformly distributed on the surface of the support, are observed, as well as the formation of some agglomerates. These results regarding the shape of the particles for the MMD2-Fe_2O_3 coincide with those α-Fe_2O_3 spherical shapes nanoparticles found by Lassoued et al. [11] and Supattarasakda et al. [12].

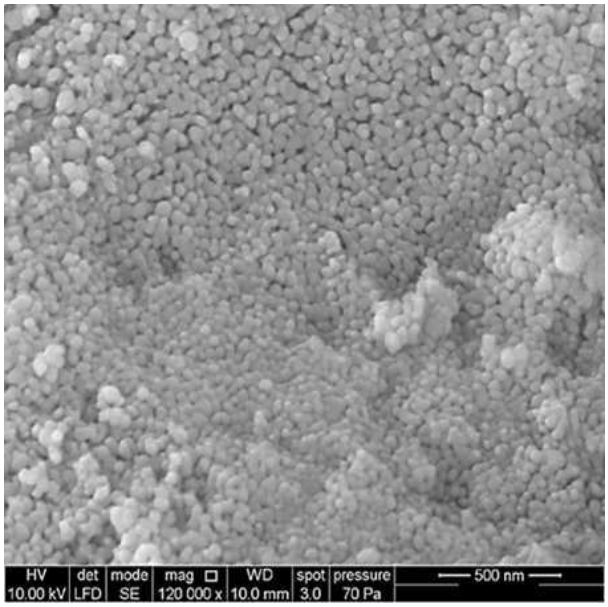

Fig. 3. SEM Image in SE mode for MMD2-Fe_2O_3.

Mass Spectrometry with Inductively Coupled Plasma (ICP-MS).

Table 1 shows the results obtained from the ICP analysis. It is observed that the obtained % Fe_2O_3 is slightly lower than the theoretical percentage used for impregnation. Pal et al. [13-14] reported similar results, in which some of the metal ions leached and did not bind with the silica species. It is possible that in this work, after the impregnation of the metals, some metal ions have undergone a leaching process, which decreased their presence in the support. On the other way, part of the material could be retained by the container.

Table 1. Mass percentage presents in mesoporous samples.

Element	Theoretical Weight %	MMD 1 (%)	MMD 2 (%)	MMD 3 (%)
Fe	10	7.96 ±0,04	7.60 ±0,04	7.98 ±0,04

Transmission Electron Microscopy.

Figure 4A shows that pure MMD1 has very visible pores within a short-range ordering while pure MMD2 (figure 4B) shows a short-range ordering with less visible pores. Pure MMD3 (figure 4C) has two types of structure, an amorphous structure and a crystalline structure. Figure 5A is a magnification of figure 4C. From figure 5A areas with a crystalline order, associated with crystallographic planes are observed. Figure 5B shows the interplanar spacing of d~ 2.76 Å or 0.276 nm obtained from HR-TEM image can be ascribed to the adjacent (555) planes corresponding to de-aluminized Y Zeolite with cubic crystallographic structure and space group F according to the crystallographic record N°00-045-0112. MMD3-Fe_2O_3 (figure 6) shows crystallographic planes (111) and (220) (in the red box) with d_{111}= 12.92 Å and d_{220}= 8.1 Å. These planes are associated with the matrix of dealuminated Y zeolite according to the crystallographic record No. 00-45-0112.

Figure 7A and 7B show the micrograph in the bright field of the MMD1-Fe_2O_3 and MMD2-Fe_2O_3 respectively. MMD1-Fe_2O_3 shows Fe_2O_3 particles with an approximately circular shape agglomerated on the support and some particles with an elongated shape. The particle size distribution obtained from micrographs (insert in figure 7A) shows a particle size of 25.5 ± 0.4 nm. In addition, the figure 7A shows the presence of short-range ordering. Figure 7B shows the TEM micrograph for the MMD2-Fe_2O_3 sample, agglomerated particles with an approximately circular shape are observed. From figure 7B the particle size was 31.0±0.4 nm.

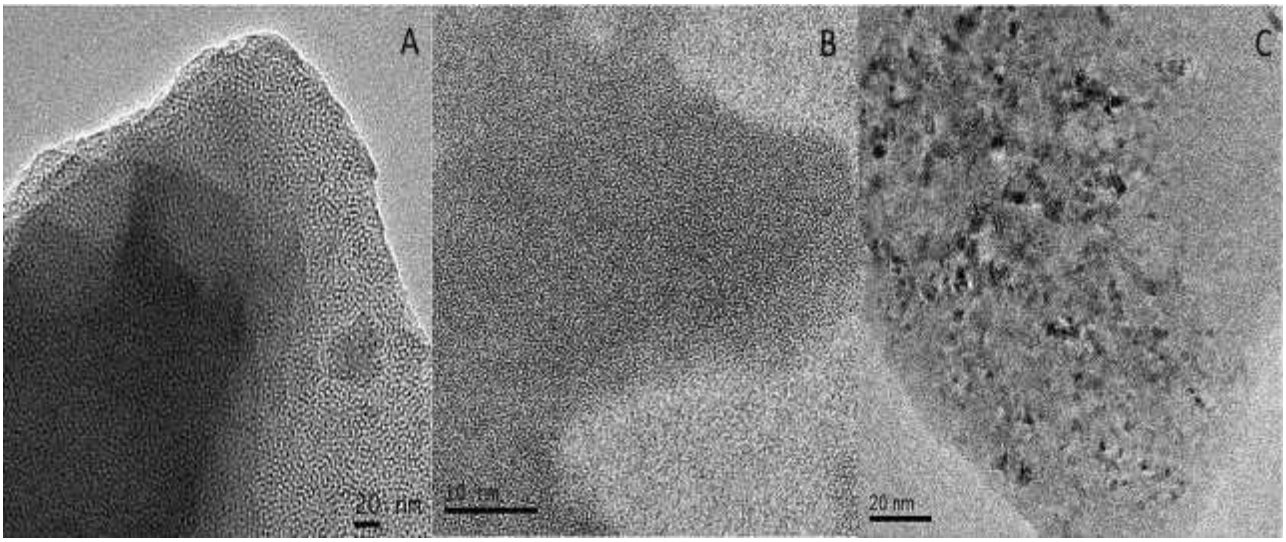

Fig. 4. TEM Image for pure MMD1 (A), pure MMD2 (B), and pure MMD3 (C).

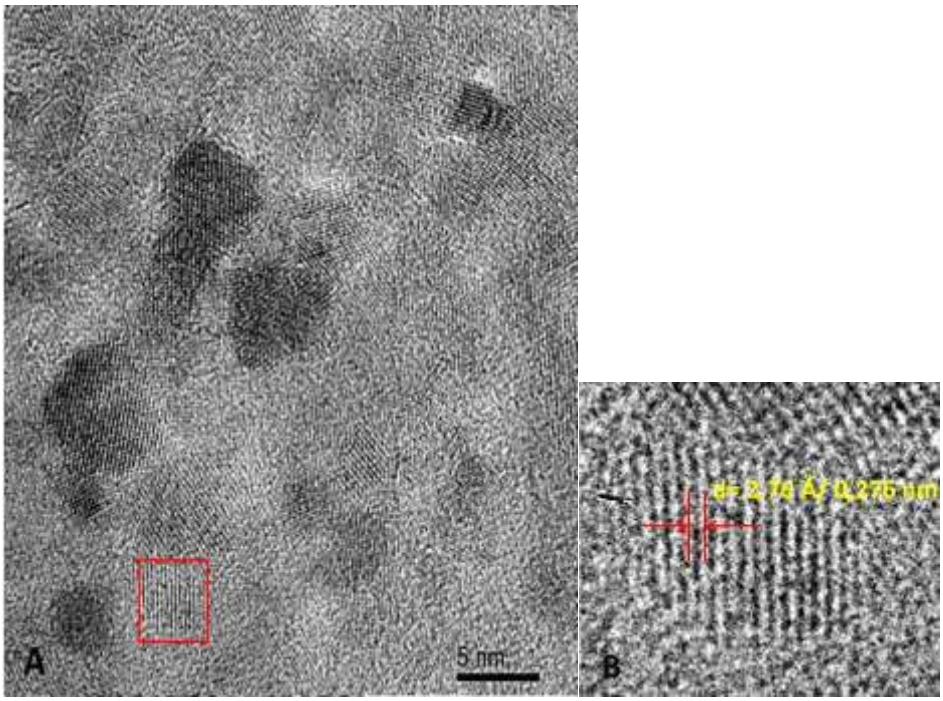

Fig. 5. HR-TEM image for pure MMD3 (A) and (B) d-spacing 2,76 Å= 0.276 nm can be ascribed to the adjacent (555) planes identified for the dealuminated Y Zeolite.

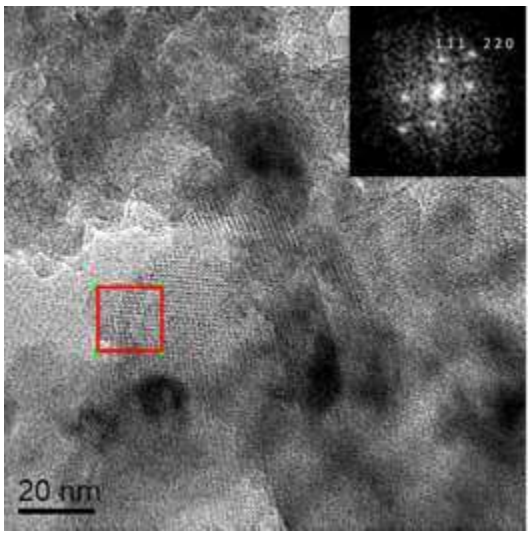

Fig. 6. TEM Image for MMD3-Fe_2O_3.

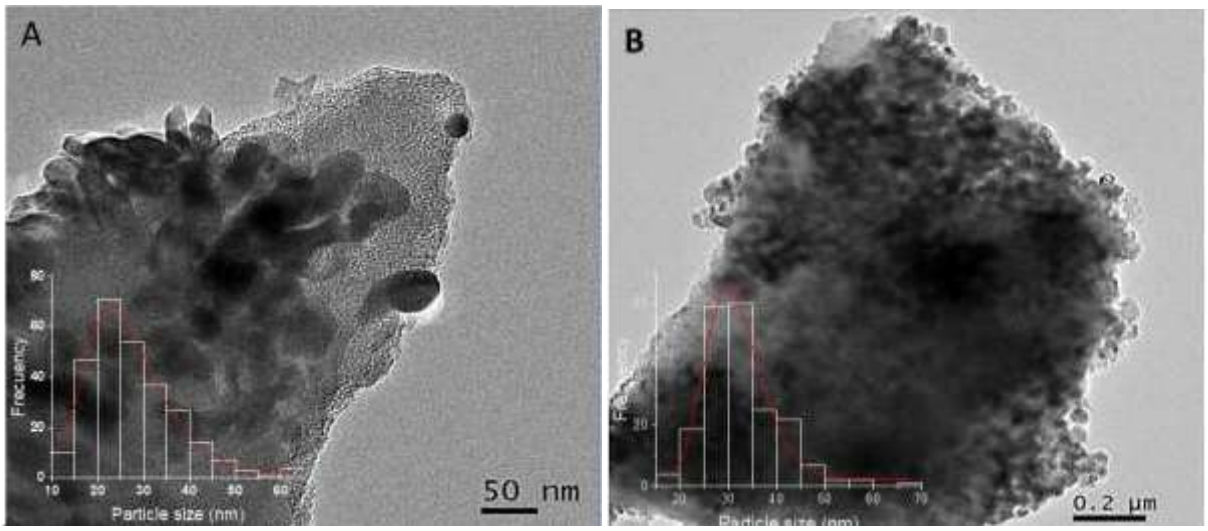

Fig. 7. TEM Image for MMD1-Fe_2O_3 and its particle size distribution (A), MMD2-Fe_2O_3 and its particle size distribution (B).

The average particle sizes obtained from the transmission micrographs for MMD1-Fe_2O_3 and MMD2-Fe_2O_3 show that both matrices have approximately similar sizes of Fe_2O_3. The difference in particle sizes is associated with the support characteristics according to Kiselev and Krylov [15]. Also, average particle size shows that Fe_2O_3 particles grow mostly outside the pore.

Textural Properties

Figure 8 shows the isotherms for pure MMD1, MMD2, and MMD3 and MMD1-Fe_2O_3, MMD2-Fe_2O_3, and MMD3-Fe_2O_3 samples. Pure MMD1 has a type I isotherm of a microporous solid. Kruk and Jaroniec [16] indicate that this type of isotherms is also observed in mesoporous materials with pore sizes close to the micropore range. The type of pore is suggested cylindrical because the type of isotherm obtained coincides with one of those reported by Kruk and Jaroniec [17]. Pure MMD2 and MMD3 shown a type IV isotherm of a mesoporous solid whose adsorption is in multilayers and with capillary condensation; they have a type H4 hysteresis characteristic of the adsorption-desorption of narrow slit type pores.

From N_2 adsorption isotherms, it can be observed that pure MMD3 material has the highest adsorption volume compared to pure MMD2 and MMD1 materials. Table 2 shows that the volume adsorbed for MMD3 is 0.972563 cm^3/g while for MMD2 and MMD1 is 0.546661 cm^3/g and 0.236739 cm^3/g, respectively. Also, table 3 shows that the adsorbed volume of N_2 and the surface area decreases with the metal oxide impregnated in the mesoporous matrix, which can be the product of two situations, one that effectively filled the pore channels and the other, that the material is blocking the entrance to the pore channel. That has an impact on a decrease in adsorbed volume [18-19], and the surface area by positioning the oxide particles inside the pore, blocking the microporosity, or the oxide particles will be placed on the surface of the support [20-22]. Figure 8 also shows that most of the isotherms keep their shape; indicating that impregnation does not modify the mesoporous support. However, the MMD3 isotherm suffered a change in the loop shape of the hysteresis after impregnation with Fe_2O_3, which indicates a partial deformation in the structure of the pores of the matrix [23]. MMD2 and MMD3 pore size distribution were determined by the BJH model (Barrett, Joyner, and Halenda) and MMD1 average pore diameter was used for comparative purposes assuming cylindrical pores [24].

Table 2 shows that the pore diameter for the MMD1 and MMD3 matrix decreases concerning to the pure support when Fe_2O_3 was incorporated, but the MMD2-Fe_2O_3 remained the same as the pure matrix; which indicate that the impregnation with the metal oxide did not influence the pore size [21, 25]. The decrease in pore size is associated with the blocking of the pores by metal particles [26].

From pore size distribution graphs of MMD2 and MMD3 (figure 9) we observe that the curves are monomodal, which is indicative of uniform pore sizes, all within the mesopore range.

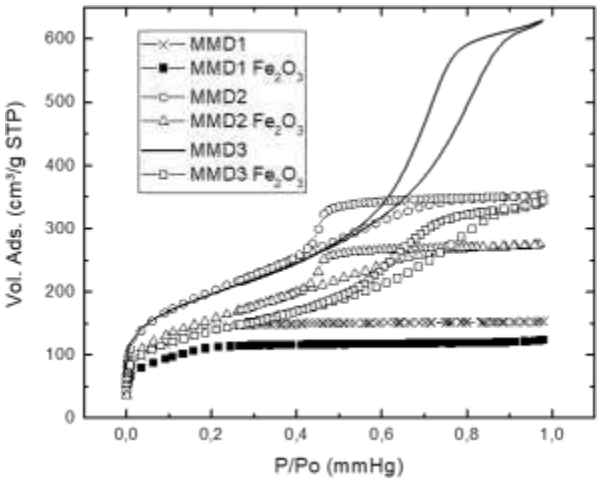

Fig. 8. N_2 adsorption isotherms for MMD1, MMD2, MMD3, MMD1-Fe_2O_3, MMD2-Fe_2O_3, and MMD3-Fe_2O_3.

The nature of the support, the structural characteristics of the three supports such as surface area, pore-volume, and pore-size, also influences the behavior of the system, namely adsorption properties. Specifically, the MMD2 and MMD3 support show greater adsorption than MMD1 since they have greater mesoporosity. Likewise, the pore structure influences the interaction of sorbate molecules and adsorption sites. A larger surface area means more adsorption sites available in the material and indicates better diffusivity of sorbate, which is important for optimal mass, and heat transfer [23]. These results show that there is a modification of the substrate due to the incorporation of the oxide.

Table 2. Textural Properties of Mesoporous Materials.

Sample	Pore Diameter (Dp) (nm)	Superficial area (m^2/g)	Vol. Ads. (cm^3/g)
MMD1	2	466	0.236739
MMD2	3.5	671	0.546661
MMD 3	6.2	664	0.972563
MMD1-Fe_2O_3	1.9	394	0.191825
MMD2-Fe_2O_3	3.5	526	0.426074
MMD3-Fe_2O_3	5.3	465	0.532317

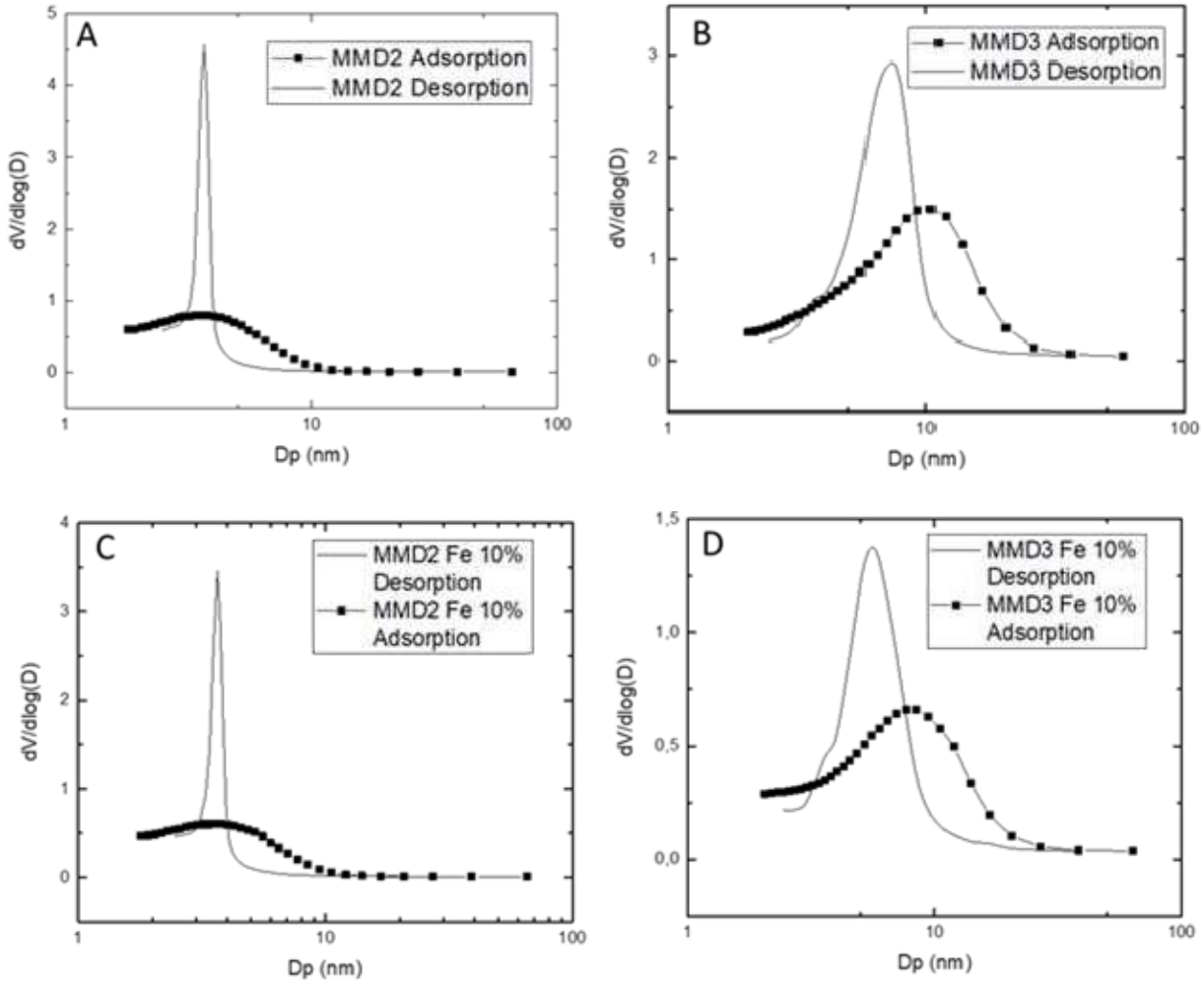

Fig. 9. Pore distribution: pure MMD2 (A), MMD3 (B), MMD2-Fe_2O_3 (C) and MMD3-Fe_2O_3 (D).

X-ray diffraction.

In figure 10 the high angle diffraction pattern for MMD1 and MMD2 are shown. The diffraction pattern for amorphous materials with a broad peak located between 2θ = 12° and 35° is observed. For MMD1-Fe_2O_3 and MMD2-Fe_2O_3 the diffraction patterns are observed; associated with Fe_2O_3 according to PDF crystallographic file No. 01-087-1166, Rhombohedral system, space group R-3c, and parameters a = 5,0353 Å and c = 13,7495Å.

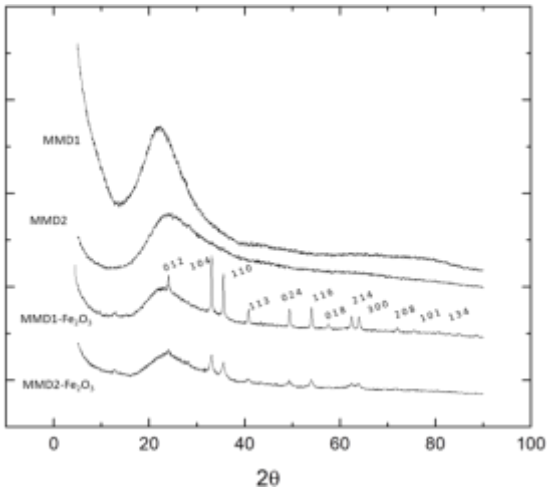

Fig. 10. Diffractograms for Pure MMD1 and MMD2, MMD1-Fe_2O_3 and MMD2-Fe_2O_3.

The intensity of the Fe_2O_3 signal for MMD1-Fe_2O_3 is associated with the high concentration of precursors on the surface of the silica matrix. The latter, caused the pore volume capacity to be insufficient to promote the growth of the metal oxide particles in confinement. Instead, the excess of the precursor was deposited on the pores. Besides, the particles also formed an external surface on the silica. These observations in accordance with the studies of a highly crystalline oxide phase identified by Zeleňak et al. [28].

In figure 11 the diffractograms for pure MMD3 and MMD3-Fe_2O_3 are shown; in this figure the same broad peak between 2θ = 12° and 35°, and some additional peaks concerning to de-aluminized Y zeolite, with a cubic crystallographic system, spatial group F, and parameter *a*=24,225 Å according to PDF No. 00-045-0112, are observed.

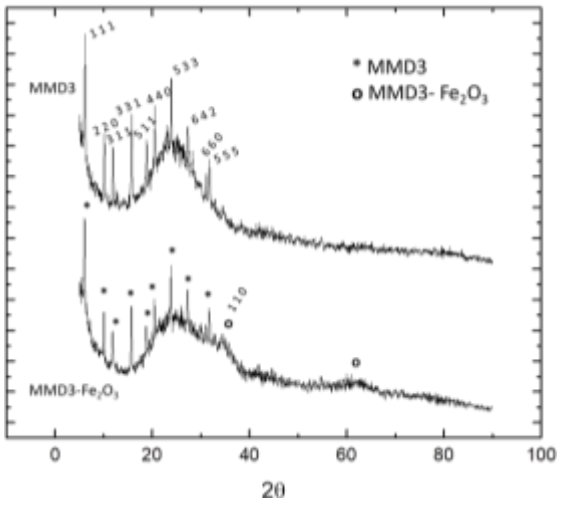

Fig. 11. Diffractograms for pure MMD3 and MMD3-Fe_2O_3.

In the MMD3-Fe_2O_3 diffraction pattern, two very small hard to detect, because of the signal-to-noise ratio, reflection peaks are observed. These peaks are corresponding to Fe_2O_3 according to PDF file No. 01-087-1166. In addition to the wide peak for the amorphous material (between 2θ = 12° and 35°), the diffraction peaks associated with the de-aluminated Y Zeolite are observed according to the PDF crystallographic file N ° 00-045-0112, with a cubic system, spatial group F and parameter *a*= 24,225 Å.

The result for the MMD3 support is similar to reported by Ali et al. [26], they impregnated a type Y zeolite with iron III at a concentration of 10%, 20% and 30% in weight and they found that the DRX for the pure zeolite shows all the peaks associated with this zeolite, while for samples impregnated with iron oxide, no signals associated with this oxide were detected.

The average crystal size for the Fe_2O_3 was calculated using the Scherrer equation 1. Table 3 shows that the average crystal size for Fe_2O_3 on MMD1 is larger than that for Fe_2O_3 on MMD2. The Fe_2O_3 on MMD3 average size could not be calculated because there is not an intense signal for the Fe_2O_3.

Table 3. Average size of the crystals obtained by DRX.

Sample	Crystals size (nm)
MMD1- Fe_2O_3	21.14
MMD2- Fe_2O_3	10.71

It can be observed that in both samples the crystals sizes are larger than the pore diameter, which suggests that the Fe_2O_3 particles could grow mostly outside the pore in both supports. Also, this analysis revealed the crystal structures of Fe_2O_3 in the supports MMD1, MMD2, and MMD3. MMD1-Fe_2O_3 was the sample with greater crystallinity following by MMD2-Fe_2O_3 with good crystallinity. However, in the sample MMD3-Fe_2O_3, Fe_2O_3 did not obtain a good crystallinity suggesting that the crystallinity of the support influences the crystallinity of iron oxide.

H_2S Adsorption Capacity Tests.

Table 4 shows the H_2S adsorption results from the different samples studied. MMD1-Fe_2O_3 was the highest adsorption with 190.26 mg of H_2S/g of adsorbent. This result is better than reported by Abatzoglou and Boivin [29] on biogas purification processes, they indicate that a

commercial product based in Fe_2O_3 and Fe_3O_4 has an adsorbent capacity of 150 mg H_2S/g adsorbent.

The adsorption process could influence the support effect that gives greater adsorption of H_2S to MMD1-Fe_2O_3 although the MMD2-Fe_2O_3 has greater surface characteristics (adsorbed volume, surface area, and pore diameter). Differences between them are associated with the shape of the pore channel of the matrix. MMD1 has cylindrical pores and MMD2 has slit type pores according to N_2 adsorption. On this point, Zhang [30] report in their H_2S removal work that textural parameters of mesoporous silica, and especially the type of the pore channel, is very important for the performance in the desulfurization process using sorbents. Also, it is observed that MMD3 decreased its H_2S adsorption capacity with impregnation. Furthermore, the results showed that when the pore size is larger, the less H_2S adsorption is. This suggests that Fe_2O_3 on the surface of the matrix also contributes to improving the capacity of H_2S adsorption when the pore size is small.

Table 4. Adsorption Capacity of H_2S Test.

Sample	Capacity adsorption (mg H_2S/gr adsorbent)
MMD1	51.28
MMD2	48.78
MMD3	69.87
MMD1-Fe_2O_3	190.26
MMD2-Fe_2O_3	98.53
MMD3-Fe_2O_3	33.66

From the results in this study, it is evidenced that MMD1 impregnated with 10% Fe_2O_3 obtained greater adsorption of H_2S compared to the other materials studied. The characteristics presented by this material, the adsorption isotherm of N_2 type I, cylindrical type pores, Fe_2O_3 particles size between 21 nm and 25 nm obtained by DRX and TEM, among other characteristics, highlighted their potential for greater capacity of adsorption. For this reason, MMD1 impregnated with 10% Fe_2O_3 could be a good option to be used in H_2S removal.

CONCLUSIONS

In this work, three amorphous mesoporous materials with different characteristics were prepared and impregnated with 10% of Fe_2O_3. They were characterized by SEM, EDX, ICP-MS, TEM, Adsorption Isotherms of N_2, DRX, and H_2S adsorption capacity tests. The results show the influence of the support on the H_2S adsorption. The pore channel type and diameter and adsorption isotherms type were the characteristics that were considered to improve H_2S adsorption. In particular, the MMD1-Fe_2O_3 which has an isothermal N_2 adsorption type I, with micro-mesopores and a cylindrical pore channel. Additionally, the average particle size for MMD1-Fe_2O_3 was determined in 25 nm by TEM, and crystal size estimated from Scherrer's formula was in good agreement with that average particle size. Also, the results suggest that superficial Fe_2O_3 contributes to improve the H_2S adsorption when the pore size is small. Because of these results, MMD1 impregnated with 10% of Fe_2O_3 could be a good option to use as an adsorbent in the removal of H_2S in various industrial processes associated with the control of environmental emissions and the improvement in the quality of oil and gas that is produced.

ACKNOWLEDGMENTS

To Universidad Central de Venezuela (UCV) and Instituto Venezolano de Investigaciones Científicas (IVIC) for supporting this investigation.

REFERENCES

[1] Li S., Li K., Hao J., Ning P., Tang L., Sun X. (2016) "Acid modified mesoporous Cu/SBA-15 for simultaneous adsorption/oxidation of hydrogen sulphide and phosphine". *Chemical Engineering Journal* 302:69-76. DOI: 10.1016/j.cej.2016.05.037.

[2] Wang X., Sun T., Yang J., Zhao L., Jia J. (2008) "Low-temperature H_2S removal from gas streams

with SBA-15 supported ZnO nanoparticles" *Chemical Engineering Journal* 142(1):48-55. DOI: 10.1016/j.cej.2007.11.013.

[3] Occupational Safety and Health Administration (OSHA). *Hydrogen Sulfide*. https://www.osha.gov/SLTC/hydrogensulfide/index.html. Accessed December 8th, 2019.

[4] Tao M., Meng X., Xin Z., Bian Z., Lv Y., Gu J. (2016) "Synthesis and characterization of well dispersed nickel-incorporated SBA-15 and its high activity in syngas methanation reaction". *Appl. Catal., A: General* 516:127-134. DOI: 0.1016/j.apcata.2016.02.019.

[5] Meléndez-Ortiz H. I., Puente-Urbina B., Castruita-de Leona G., Mata-Padilla J. M., García-Uriostegui L. (2016) "Synthesis of spherical SBA-15 mesoporous silica. Influence of reaction conditions on the structural order and stability" *Ceram. Int.* 42(6):7564-7570.DOI: 10.1016 /j.ceramint.2016 .01.163.

[6] Vahid A., Qandalee M., Baniyaghoob S. (2017) "H_2S removal using ZnO/SBA-3: New synthesis Route and Optimization of Process Parameters". *Scientia Iranica C* 24(6), 3064-3073. DOI: 10.24200 /SCI. 2017.4573.

[7] Mohammed Ali G. A., Barhoum A., Kumar Gupta V., Ahmed Nada A., Hassan El-Maghrabi H., Kanthasamy R., Ramadan Shaaban E., Algarni H., Feng Chong K. (2020) "High surface area mesoporous silica for hydrogen sulfide effective removal". *Curr. Nanosci.* 16(2):226-234 DOI: 10.2174/1573413715666181205122307.

[8] Li S., Liu Y., Gong H., Wu K.-H., Ba H., Duong-Viet C., Jiang C., Pham-Huu C., Su D. (2019) "N-Doped 3D Mesoporous Carbon/Carbon Nanotubes Monolithic Catalyst for H_2S Selective Oxidation" *ACS Appl. Nano Mater.* 2(6):3780−3792. DOI: 10.1021/acsanm.9b00654.

[9] Li L., Sun T. H., Shu C. H., Zhang H. B. (2016) "Low temperature H_2S removal with 3-D structural mesoporous molecular sieves supported ZnO from gas stream" *J. Hazard. Mater*. 311:142–150. DOI: 10.1016/j.jhazmat.2016.01.033.

[10] Goldstein J., Newbury D. E., Michael J. R., Ritchie N. W. M., Scott J. H. J., Joy D. C. (2007) "*Scanning Electron Microscopy and X-Ray Microanalysis"* 3rd ed. New York: Editorial Springer. p. 141.

[11] Lassoued A., Dkhil B., Gadri A., Ammar S. (2017) "Control of the shape and size of iron oxide (α-Fe2O3) nanoparticles synthesized through the chemical precipitation method". *Results in Physics* 7:3007–3015. DOI: 10.1016/j.rinp.2017.07.066.

[12] Supattarasakda K., Petcharoen K., Permpool T., Sirivat A., Lerdwijitjarud W. (2013) "Control of hematite nanoparticle size and shape by the chemical precipitation method" *Powder Technol.* 249:353–359. DOI: 10.1016/j.powtec.2013.08.042.

[13] Pal N., Im S., Cho E.-B., Kim H., Park J. (2019) "Superparamagnetic NiO-doped mesoporous silica flower-like microspheres with high nickel content" *Journal of Industrial and Engineering Chemistry* 81:99-107. DOI: 10.1016/j.jiec.2019.08.058.

[14] Pal N., Kim T., Park J.-S., Cho E.-B. (2018) "Synthesis of ordered Ca- and Li-doped mesoporous silicas for H_2 and CO_2 adsorption at ambient temperature and pressure" *RSC Adv*. 8:35294-35305. DOI: 10.1039/C8RA05772A.

[15] Kiselev V. F., Krylov O. V. (1989*)* "*Adsorption and Catalysis on Transition Metals and Their Oxides. Springer Series in Surfaces Sciences 9*" Heidelberg: Editorial Springer-Verlag. p.p.445. DOI:10.1007/978-3-642-73887-6.

[16] K. M., Jaroniec M. (2001) "Gas Adsorption Characterization of Ordered Organic-Inorganic Nanocomposite Materials" *Chem. Mater*. 13(10):3169-3183. DOI: 10.1021/cm0101069.

[17] Kruk M., Jaroniec, M. (2000) "Accurate Method for Calculating Mesopore Size Distributions from Argon Adsorption Data at 87 K Developed Using Model

MCM-41 Materials". *Chem. Mater*. 12(1):222-230. DOI: 10.1021/cm9905601.

[18] Khalil S. H. (2018) "Effects on Surface Area, Intake Capacity and Regeneration of Impregnated Palm-Shell Activated Carbon with Monoethanolamide and 2-Amino-2-Methyl-1-Propanol Equipped for CO_2 Adsorption" *Earth Sci. Clim. Change* 9(7):484. DOI: 10.4172/2157-7617.1000484.

[19] Xu Q.-Q., Yin J.-Z., Zhou X.-L., Yin G.-Z., Liu Y.-F., Cai P. Wang A.-Q. (2016) "Impregnation of Ionic Liquids in Mesoporous Silica Using Supercritical Carbon Dioxide and Co-solvent" *RSC Adv*. 6:101079-101086. DOI: 10.1039/C6RA20287J.

[20] Hidayu A. R, Muda N. (2016) "Preparation and characterization of impregnated activated carbon from palm kernel shell and coconut shell for CO_2 capture" *Procedia Engineering*. 148:106 – 113. DOI: 10.1016/j.proeng.2016.06.463.

[21] Dewajani H., Rochmadi, Purwono S. Budiman A. (2016) "Effect of modification ZSM-5 catalyst in upgrading quality of organic liquid product derived from catalytic cracking of Indonesian nyamplung oil (Calophyllum inophyllum)". *AIP Conference Proceedings* 1755(1):050002. DOI: 10.1063/1.4958485.

[22] Silveira E. B., Veloso C. O., Costa A. L. H., Henriques C. A., Zotin F. M. Z., Paredes M. L. L., Reis R. A., Chiaro S. S. X. (2015) "Influence of Metal Oxides Impregnated on Silica–Alumina in the Removal of Sulphur and Nitrogen Compounds from a Hydrotreated Diesel Fuel Stream" *Adsorpt. Sci. Technol*. 33(2). DOI: 10.1260/0263-6174.33.2.105.

[23] Ristic A. Zabukovec Logar N. (2019) "New Composite Water Sorbents $CaCl_2$-PHTS for Low-Temperature Sorption Heat Storage: Determination of Structural Properties" *Nanomaterials* 9(1):27. DOI: 10.3390/nano9010027.

[24] Marczewski A.W. (2015) "A Practical Guide to Isotherms of Adsorption on Heterogeneous Surfaces" http://adsorption.org/awm/ads/meso/RIB-ASAP.htm. Accessed september 2nd, 2019.

[25] Chermahini A. N., Assar M. (2019) "Production of n-butyl levulinate over modified KIT-6 catalysts: comparison of the activity of KIT-SO_3H and Al-KIT-6 catalysts". *J. Iran. Chem. Soc*. 16:2045–2053. DOI: 10.1007/s13738-019-01677-4.

[26] Ali Sem S., Mohd Zabidi N., Duvvuri S. (2011) "Effect of loading on the physicochemical properties of alumina suppoted Co/Mo bimetallic nanocatalysts" *Journal of Applied Sciencies*. 11(7):1421-1425. DOI: 10.3923/jas.2011.1421.1425.

[27] Ayoub H., Roques-Carmes T., Potier O., Koubaissy B., Pontvianne S., Lenouvel A., Guignard C., Mousset E, Poirot H., Toufaily J., Hamieh T. (2018) "Iron-impregnated zeolite catalyst for efficient removal of micropollutants at very low concentration from Meurthe river" *Environ. Sci. Pollut. Res*. 25:34950-34967. DOI: 10.1007/s11356-018-1214-0.

[28] Zeleňak Vl., Zeleňáková A., Kapusta O., Hrubovčák P., Girman V., Bednarčík J. (2019) "Fe_2O_3 and Gd_2O_3 nanoparticles loaded in mesoporous silica: insights into influence of NPs concentration and silica dimensionality" *RSC Adv*. 9(7):3679-3687. DOI: 10.1039/c8ra05576.

[29] Abatzoglou N., Boivin S. (2009) A review of biogas purify cation processes. *Biofuels. Bioprod. Biore*fin. 3(1):42–71. DOI: 10.1002/bbb.117.

[30] Zhang Z. F., Liu B. S., Wang F., Wang W. S., Xia C., Zheng S., Amin R. (2014) Hydrogen sulfide removal from hot coal gas by various mesoporous silica supported Mn_2O_3 sorbents. *Appl. Surf. Sci.* 313:961–969. DOI: 10.1016/j.apsusc.2014.06.116.